Available online at www.sciencedirect.com
ScienceDirect
Ocean Modelling 17 (2007) 277–299
Ocean Modelling
www.elsevier.com/locate/ocemod

Modelling of a medium-term dynamics in a shallow tidal sea, based on combined physical and neural network methods

Agnieszka Herman *, Ralf Kaiser, Hanz D. Niemeyer

Coastal Research Station, Lower Saxony Water Management, Coastal Defence and Nature Conservation Agency, An der Mühle 5, 26548 Norderney, Germany

Received 2 August 2006; received in revised form 23 February 2007; accepted 26 February 2007
Available online 12 March 2007

Abstract

The paper presents an approach towards a medium-term (~decades) modelling of water levels and currents in a shallow tidal sea by means of combined hydrodynamic and neural network models. The two-dimensional version of the hydrodynamic model Delft3D, forced with realistic water level and wind fields, is used to produce a two-year-database of water levels and currents in the study area. The linear principal component analysis (PCA) of the results is performed to reveal dominating spatial patterns in the analyzed dataset and to significantly reduce the dimensionality of the data. It is shown that only a few principal components (PCs) are necessary to reconstruct the data with high accuracy (over 95% of the original variance). Feed-forward neural networks are set up and trained to effectively simulate the leading PCs based on water level and wind speed and direction time series in a single, arbitrarily chosen point in the study area. Assuming that the spatial modes resulting from the PCA are 'universally' applicable to the data from time periods not modelled with Delft3D, the trained neural networks can be used to very effectively and reliably simulate temporal and spatial variability of water levels and currents in the study area. The approach is shown to be able to accurately reproduce statistical distribution of water levels and currents in various locations inside the study area and thus can be viewed as a reliable complementary tool e.g., for computationally expensive hydrodynamic modelling. Finally, a detailed analysis of the leading PCs is performed to estimate the role of tidal forcing and wind (including its seasonal and annual variability) in shaping the water level and current climate in the study area.

Keywords: Tidal inlets; Hydrodynamic modelling; Principal component analysis; Neural networks; North Sea; Wadden Sea; East Frisian Islands

1. Introduction

The investigation of many important aspects of the coastal zone processes – e.g., the analysis of sediment transport or studies concerning the safety of various coastal protection structures and the coast itself – is

* Corresponding author. Present address: Institute of Oceanography, University of Gdańsk, Pilsudskiego 46, 81-378 Gdynia, Poland. Tel.: +48 58 523 6879.
E-mail address: herman@ocean.univ.gda.pl (A. Herman).

1463-5003/$ - see front matter © 2007 Published by Elsevier Ltd.
doi:10.1016/j.ocemod.2007.02.004

possible only if data concerning medium-term (∼decades) variability of waves and currents in the study area are available. Because of enormous costs and technical difficulties of long-term measuring campaigns on the one hand, and typical shortage of input data required by (usually extremely computationally expensive) numerical models on the other hand, the knowledge of temporal and spatial variability of waves and currents in the coastal zone is usually very limited.

The work presented in this study is part of a research project MOSES (“Modelling of the medium-term wave climatology at the German North Sea coast”), one of the purposes of which is to produce a medium-term database of water levels, currents and mean wave parameters for a coastal area in the German Wadden Sea. Although the state-of-the-art hydrodynamic and wave models are able to reproduce the wave and current processes in shallow tidal seas with high accuracy, their application to medium-term modelling is limited because of enormous computer resources that are required to reach spatial and temporal resolution sufficient to resolve all details of the complicated geometry of the coastal zone. The methods typically used to address these problems, e.g., nesting or grids with varying spatial resolution, only in some cases provide a satisfactory solution. Moreover, the amount of data produced by the models makes their direct usage in further applications (e.g., as input for morphodynamic modelling) practically impossible. Therefore, even if one is able to conduct sufficiently long simulations, additional data analysis tools are necessary, enabling the reduction of the amount of data without loss of information crucial for the understanding of the processes analyzed and for further application of the modelling results.

In the present study the results of high-resolution hydrodynamic simulations of water levels and currents (wave modelling in the study area will be treated in detail elsewhere) are used as a starting point for the development of a neural network-based modelling system, which enables fast and sufficiently accurate hindcasting of temporal and spatial patterns of water levels and currents in the study area. The main idea behind the approach developed is to decompose the dataset into a (small) number of fixed modes, assumed ‘universal’ over the four decades studied, and to model the time variations of those modes only, thus reducing the dimensionality of the problem by more than three orders of magnitude. The results presented in this paper show that the assumption of the medium-term ‘universality’ of the modes is justified. Contrary to the earlier works concerning neural network modelling of tides, e.g., by Lee and Jeng (2002), Huang et al. (2003) (see also the review of neural network applications given in this work) or Lee (2004), the approach used here enables to reproduce water levels and currents *in the whole study area*, not only at single stations as in the cited papers. The results presented indicate that the principal component analysis of the results of hydrodynamic modelling is a promising input-reduction tool e.g., for morphodynamic and other studies (as suggested by de Vriend et al., 1993), for which the knowledge of the temporal and spatial variation of water levels and currents is a prerequisite. The idea behind the PCA/NN technique used here is in many aspects similar to the one of Álvarez et al. (2000), who applied PCA combined with genetic algorithms to forecast the space-time variability of the satellite-derived monthly sea surface temperature fields in the western Mediterranean Sea. Similarly, Álvarez (2007) used the combination of the complex PCA (CPCA) and genetic algorithms to the analysis of propagating thermal fronts.

The structure of the paper is as follows: in the next section a description of the study area is given, followed in Section 3 by a description of the hydrodynamic model Delft3D used in the simulations. The verification of the results is presented as well. Section 4 discusses the results of the linear principal component analysis (PCA) of water levels and currents, with emphasis given to aspects crucial for the further stages of the project realization. The results of PCA, together with time series of water level and wind velocity components in a chosen location, are then used to set up and train a feed-forward neural network (NN), as described in detail in Section 5. The trained NN is shown to accurately reproduce the test data and hence to be applicable as a tool for producing the data in periods that could not be modelled with Delft3D because of time constraints. In Section 6 the influence of wind and its seasonal and annual variability on the water level and current climate in the study area is investigated. Finally, Section 7 summarizes and discusses the results.

2. Area description

The main object of the study are the catchment areas of the tidal inlets between the islands of Borkum, Juist and Norderney, belonging to the chain of the East Frisian Islands separating the German Wadden Sea from

the North Sea. The location of the study area, together with its bottom topography, is shown in Fig. 1. All morphological features typical for this coast type can be identified in the water basins analyzed: tidal flats, covering most of the basins areas, and single or multiple channels providing connection with an open sea. The main parameters describing the geometry of the basins – their surface area at the mean water level, average water depth, length and cross-sectional profile of the inlets etc. – vary significantly from basin to basin. However, certain functional dependence between most of these parameters can be formulated, as described in a classical work of O'Brien (1967) or – for the basins of the German Wadden Sea – by Schroeder et al. (1994) and Niemeyer et al. (1995). The importance of the above-mentioned variability and regularities from the point of view of the hydrodynamics and the water transport through the system has been addressed recently e.g., by Stanev et al. (2003a,b) and Herman (2007b). The strong dependence of the basins' volumes, surface areas and the cross-sectional profiles of the inlets on the water level is well known to be one of the main sources of strongly nonlinear behaviour of the tidal systems.

The amplitudes of the three most energetic tidal components M2, S2 and N2 vary from 94 cm, 26 cm and 16 cm at the entrance to the inlet between Borkum and Juist to 106 cm, 28 cm and 17 cm, respectively, at the entrance to the inlet between Norderney and Baltrum (values based on the long-term modelling results with the Delft3D model; see next section). The phase lag between the two above locations equals for all three

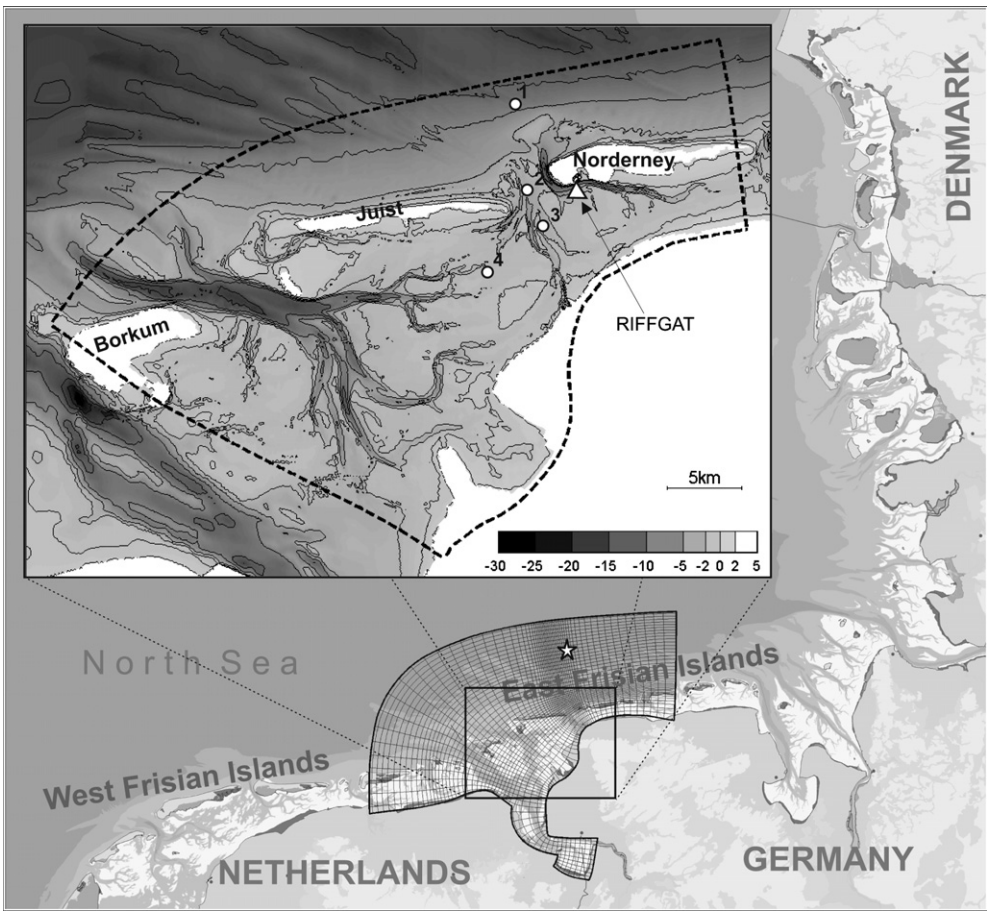

Fig. 1. Location of the study area on the German North Sea coast. Continuous lines in the large panel show the curvilinear grid of the Delft3D model (every 10th line in each direction), the star – the location of an input point for the wind atlas and the NN modelling (see text for detailed description). In the small panel the bathymetry (in meter relative to the German datum) of the study area is shown. The dashed line marks the boundary of the region, in which the results are analyzed and modelled with PCA/NNs. The triangle shows the location of the water level station RIFFGAT. Points 1–4 show the locations, in which the statistical distribution of water levels and currents is analyzed (Supplementary material to Section 5).

components ~24°. Yearly mean wave heights seawards from the inlets are slightly lower than 1 m. According to the classification of Hayes (1979) the region is subject to upper mesotidal conditions. Although the tidal forcing is the dominating factor shaping the hydrodynamic phenomena in the study area, the spatial and temporal variability of water levels and currents can be significantly modified by (especially north-westerly) winds, see further Section 6 and Herman (2007b).

3. Description and verification of the model

As mentioned in Section 1, the work presented here is part of a larger project, the main purpose of which is to produce a medium-term database (1962–2002, time range in which the input data are available; see below) of water level, current and wave data for the area under interest. The hydrodynamic modelling is performed by means of the two-dimensional (2D) version of the Delft3D model (Roelvink and van Banning, 1994; Delft Hydraulics, 2003), based on depth-averaged momentum and continuity equations. Comparisons between the results of the 2D and 3D model runs in a three-month-test period 09–11.2002 showed the ability of the 2D version to reproduce the water levels and the vertically-integrated currents with high accuracy: the differences between the two model runs remained within 2–4 cm for water levels (with slightly higher values at low water – the 2D version tends to produce slightly higher low water levels) and within 2–5 cm/s for currents, independently on wind conditions. Thus, the use of the 2D Delft3D version instead of the computationally expensive 3D version is justified (and is a common practice in tidal modelling over longer periods of time). No temperature and salinity variations have been taken into account in this study – strong tidal mixing and small water depths in the study area make any density-related effects negligible. The Reynold's stresses in Delft3D are determined using the eddy viscosity concept; the Reynold's stress tensor is assumed to be anisotropic, with the horizontal eddy viscosity coefficient (assumed constant within the study area) much larger than its vertical counterpart (Delft Hydraulics, 2003).

The model equations are formulated in orthogonal curvilinear coordinates, discretized onto a staggered Arakawa-C grid and time-integrated by means of an ADI (alternating direction implicit) numerical scheme. For the modelling in shallow tidal seas one of the most crucial features of Delft3D is the flooding/drying scheme. Because of the importance of robust and accurate modelling of drying and flooding of tidal flats for our purposes, various test model runs have been performed with different values of the parameters governing the functioning of the flooding/drying algorithm, including the minimal water depth for which a grid point is considered 'wet', methods of interpolation of water level and depth to different corners/sides of grid cells of the staggered grid etc. (for details see Delft Hydraulics, 2003). All tests gave very similar results, showing that the algorithm functions robustly in relatively broad range of values of the above-mentioned parameters. Further in the study the set of parameters has been used for which the spurious water-level fluctuations generated by drying/flooding were minimal. A brief summary concerning the model setting is provided in Table 1.

The simulations have been performed on a curvilinear grid with a spatial resolution varying from ~50 m in the inlet between Juist and Norderney (called Norderneyer Seegat; the main area of interest within the MOSES project) to ~300 m at the north-western model boundary (Fig. 1). The time step has been set to 0.5 min. The model has been driven by interpolated time series of the free surface elevation at the open

Table 1
Some parameters concerning the setup of the Delft3D model for the study area (see Delft Hydraulics, 2003, for details)

Parameter	Value
Time step	30 s
Wind stress coefficient	From 0.00063 at 0 m/s to 0.00723 at 100 m/s
Bottom roughness formulation	Chezy, roughness coef. 65.0 $m^{1/2}/s$
Drying/flooding scheme	Minimum water depth: 10 cm
	Depth at water level points: MAX method
	Marginal depth in shallow areas: −999.0 m
Horizontal eddy viscosity	1.0 m^2/s
Horizontal eddy diffusivity	10.0 m^2/s

boundary and by space- and time-varying winds. All input data (hourly fields of water level and wind velocity components on a $0.1° \times 0.05°$-grid in geographical coordinates) have been extracted from the dataset produced within the European Union project HIPOCAS (Hindcast of Dynamic Processes of the Ocean and Coastal Areas of Europe; Weisse et al., 2002) and covering the period 1962–2002. The HIPOCAS project aimed at generating a consistent hydrodynamic dataset for the North Sea, applicable as a source of boundary conditions for small-scale coastal models. The HIPOCAS data have been shown to reproduce the statistical distribution of the analyzed quantities with high accuracy. From the point of view of the present study it is important to notice that there are no trends in the water level data. The variability of the HIPOCAS winds is more complex: although no trends are present, an increasing occurrence frequency of strong wind events in the cold time of the year can be noticed (see Section 6); however, for this study changes in the *course*, not the *frequency* of wind events are important. No such changes could be found in the analysis of the HIPOCAS wind data.

Because of the coarse resolution of the HIPOCAS data the wind fields it provides are almost uniform (both in terms of magnitude and direction) over the whole study area. To increase the quality of the wind data over the Wadden Sea (sheltering effects of the islands, variations in the roughness coefficient due to drying/flooding of the tidal flats etc.), the wind fields used as input for Delft3D have been produced from HIPOCAS time series in a point marked with a star in Fig. 1 by means of the wind atlas of the German Meteorological Service (DWD). The wind atlas had been produced within MOSES and designed to fit its purposes. It contains high-resolution unidirectional wind fields for a number of wind speed, wind direction and water level classes, calculated by means of a wind model in which variations of the surface friction due to drying/flooding of the tidal flats and due to changes in sea state (estimated by a simple statistical wave model) have been taken into account.

The applicability of Delft3D to modelling of the Wadden Sea hydrodynamics has been proved in numerous studies performed by the Coastal Research Station and others, see e.g. Roelvink and van Banning (1994), Luijendijk (2001) or Delft Hydraulics (2001). Within MOSES the verification of the modelling results has been performed at a station RIFFGAT to the south of the island of Norderney (triangle in Fig. 1) in the period September–November 2002. Fragments of the measured and modelled time series of water levels are shown in Fig. 2. As can be seen, the model performance is satisfactory, although the low water levels tend to be overestimated (on average by 17 cm) and the high water levels underestimated (on average by 9 cm). There is also a phase shift of about 40 min between the two time series, which is present in the boundary data as well (see Table 2). It must be of course taken into account by modelling of the particular storm events etc., but its presence is not crucial for the statistical analysis of medium- and long-term modelling results.

In the following, the results of the Delft3D simulations from the first two years of the analysis period, 1962–1963, are used to develop a statistical model (based on PCA and NN) of the hydrodynamics of the study area.

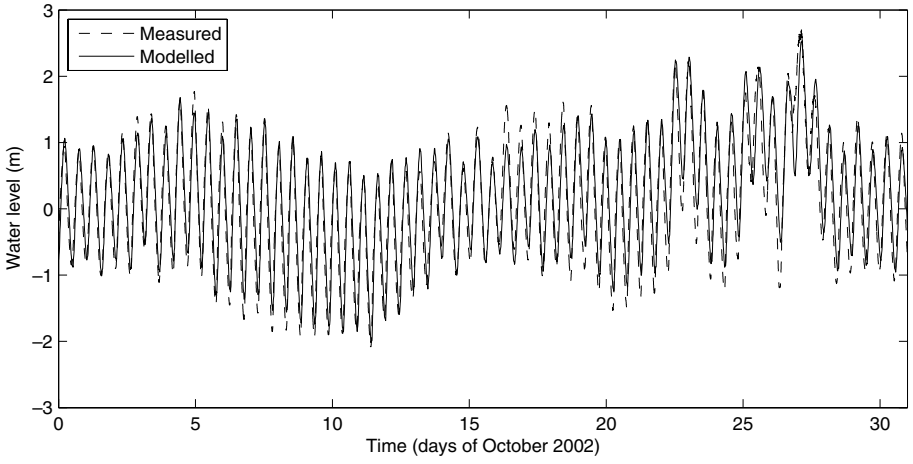

Fig. 2. Time series of measured and modelled water level at the station RIFFGAT (location see Fig. 1) in October 2002.

Table 2
Statistics of the modelled water levels at the station RIFFGAT in September–November 2002

Phase shift (min)	0	40
Correlation coefficient (%)	93	98
Std. dev. of differences (m)	0.35	0.16
Mean difference (m)	−0.04	−0.02

The applicability of the trained neural networks is then tested by comparing their predictions with the Delft3D results from the years 1985 and 2002. To eliminate the possibility that the choice of the particular years for the PCA analysis could have an influence on the performance of our modelling system (as the interannual and seasonal wind variability discussed in Section 6 could suggest) we repeated the whole procedure starting with the 1985 data and verifying the results for the 1962 data. The differences between the modes were insignificantly small and the overall performance was comparable with the one presented below. We therefore do not discuss this problem further.

4. Principal component analysis of the modelling results

The modelled water level and current fields have been saved hourly and will be analyzed further inside an area marked with a dashed line in Fig. 1. Every 5th grid point in each direction has been taken into account, resulting in $N_p \times N_t$-point data matrices of water levels $\mathbf{W} = [W_{pt}]$ and currents $\mathbf{V} = [U_{pt}] + i[V_{pt}]$, where $N_p = 3454$ is the number of data points (only those points, which remained wet during at least 10% of the simulation time have been taken into account) and $N_t = 17{,}521$ is the number of time points (hourly from 01.01.1962, 00:00 to 01.01.1964, 00:00). U and V denote the cartesian components of the current velocity vector and $i = \sqrt{-1}$ is the imaginary unit. As described in Section 2, tidal flats, falling dry at low water levels, cover considerable part of the study area. This results in a certain amount of 'exception' values in the analyzed datasets. For the purpose of the further analysis those values have been replaced with zeros in the currents matrix and with bottom level values in the water level matrix (to avoid discontinuities in the time series). The considerable amount of locations falling dry at low water was the reason why the area-mean-values were not removed from the data prior to the PCA, as is a common practice e.g., in similar studies concerning climate data. Thus, we analyze water levels and currents themselves and not their anomalies. Theory and technical details concerning PCA can be found in a number of textbooks, e.g., in Preisendorfer (1988).

4.1. PCA of water levels

As shown in Table 3, the first linear mode of water levels explains over 97% of the total variance of the data record analyzed. The first three modes are enough to reproduce over 99.6% of the variance. The spatial

Table 3
Percentage of total variance explained by the first ten linear modes of water levels and currents

	Water levels		Currents	
Mode	Separate	Cumulative	Separate	Cumulative
1	97.177	97.177	84.471	84.471
2	1.803	98.980	7.263	91.734
3	0.638	99.618	1.966	93.699
4	0.144	99.762	1.508	95.208
5	0.052	99.814	0.677	95.885
6	0.034	99.848	0.535	96.419
7	0.029	99.877	0.403	96.823
8	0.023	99.900	0.290	97.113
9	0.017	99.917	0.229	97.342
10	0.012	99.929	0.202	97.544

patterns given by those three modes are shown in the left panels of Fig. 3 (note different color scales in the panels; the modes have been scaled so that all components have a unit standard deviation). As can be seen,

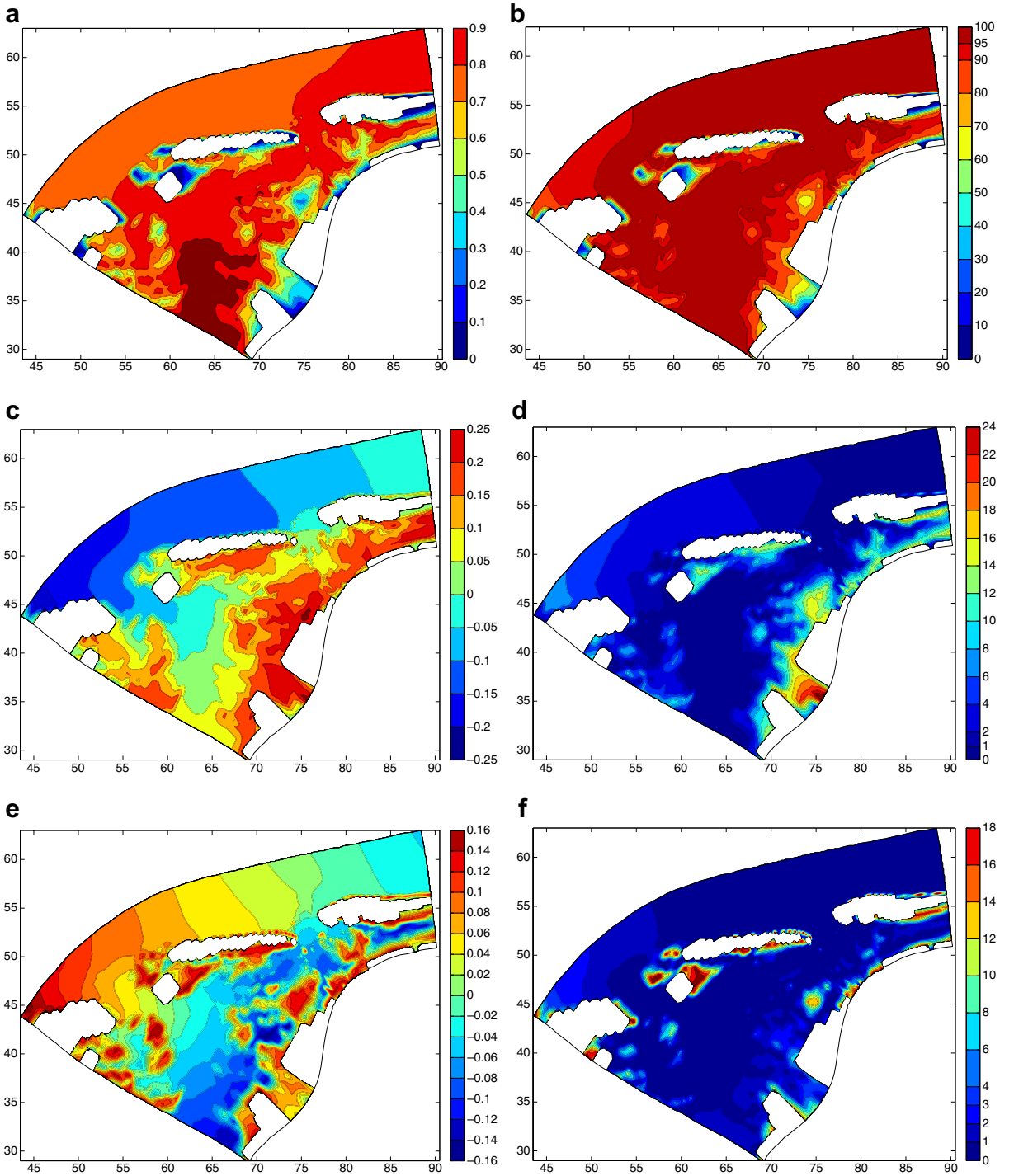

Fig. 3. Results of PCA of water levels from the period 1962–1963: spatial patterns (modes) related to the three most energetic PCs (a, c, and e) and spatial distribution of the percentage of variance explained by these modes (b, d, and f). Note different color scales in the figures. Axes labelling in km. (For interpretation of the references to color in this figure legend, the reader is referred to the web version of this article.)

the first mode and the associated principal component ($PC_{wl,1}$) represent to a high degree the variation of the average water level in the study area. This mode has positive values in all grid points. Seawards from the islands and in the channels those values vary only slightly, only in shallowest and furthest from the open boundary situated locations they are significantly lower than elsewhere. These are the locations where the percentage of variance explained by the first mode (defined as the squared correlation coefficient between the PC and the time series in a given point) is lower than 90% (Fig. 3b).

The second and third mode (Fig. 3c and e) are responsible for the alongshore water level gradient seawards from the islands, corresponding to the propagation of the tidal signal along the coast, as well as for the water level gradients in the inlets and along the channels, corresponding to the propagation of the tide into/out of the basins during flood/ebb. Those two modes (and the further ones, not shown in the figures, as well) have higher spatial variability than the first one and are important only locally (Fig. 3d and f). The five leading modes together explain over 99% of the variance in 93% of grid points and over 97% of the variance in 97% of grid points (Fig. 4a). The standard deviation of differences between the original and the reconstructed (with $PC_{wl,1}$–$PC_{wl,5}$) dataset varies between 3 and 4 cm to the north of the islands to 6 and 8 cm over most of the tidal flats (Fig. 4b), only in some isolated locations it is slightly higher. The highest values occur in the very shallow bay (Ley Bay) at the coast, a considerable part of which lies above the mean water level (Fig. 1). Thus, the water level time series there consist of long periods with constant values, which can be reproduced with sufficient accuracy only with a prohibitively large number of PCs (a problem analogous to the Fourier analysis of piecewise-constant functions; see also the next section).

The interpretation of the role of the first mode given above is confirmed by a strong relationship between $PC_{wl,1}$ and HIPOCAS water level in the chosen point, as shown in Fig. 5a. The correlation coefficient between the two time series equals 99.7%. Moreover, for water levels higher than ~0 m the relationship is almost linear. As can be expected, the nonlinear behaviour of the system manifests itself more strongly when water depths are lower and the bottom topography, friction etc. play the dominant role. As can be seen from the time variability associated with the first three leading modes of water levels presented in Fig. 5b, the tidal signal is strongly present not only in $PC_{wl,1}$, but in the further ones as well – splitting of the 'information' associated with single processes among several modes is a typical feature of the linear PCA. As will be shown in Section 6, all mode/PC pairs are a complicated mixture of signals due to the tidal and wind forcing.

The existence of nonlinear relationships between the linear PCs of water levels manifests itself in the phase diagrams of the data in the space spanned by the PC_{wl}s, see Herman (2007a). Although the PC_{wl}s are – by construction – linearly independent, there exists statistical interdependence between them (in other words, their joint probability distribution is not equal to the product of the probability distributions of single PC_{wl}s).

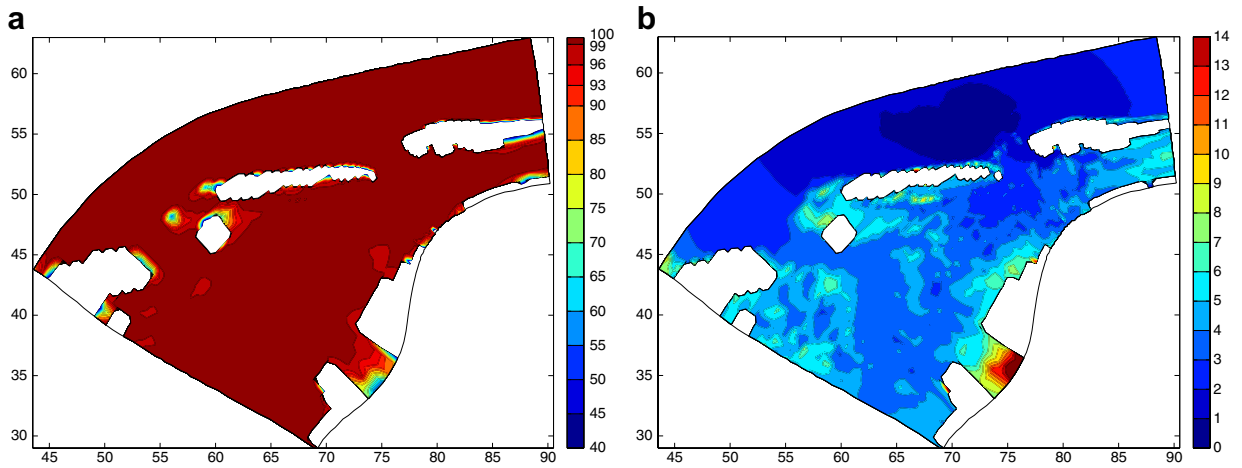

Fig. 4. Spatial distribution of the percentage of variance explained by the first five PCs (a) and of the standard deviation of differences (in cm) between the original and reconstructed with five PCs water level data (b). Axes labelling in km.

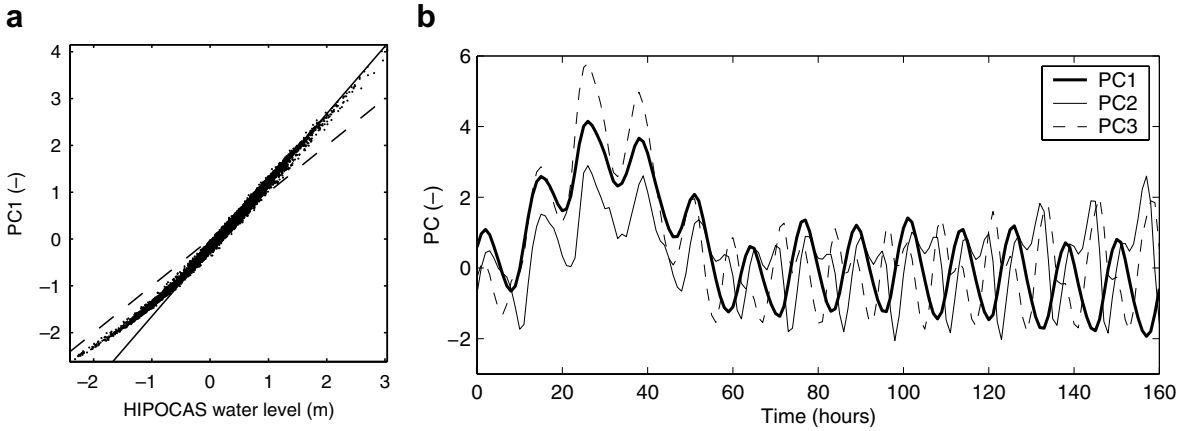

Fig. 5. (a): Dependence of the first PC of water level on the HIPOCAS water level in the point marked with a star in Fig. 1. Continuous line: best fit for HIPOCAS water levels greater than 0; dashed line: identity function. (b): Fragments of the first three leading PCs of water level.

These statistical relationships, together with the dependence of $PC_{wl,1}$ on the HIPOCAS water levels (Fig. 5a), are obviously very important from the point of view of the NN modelling, discussed further.

4.2. PCA of currents

The first three linear modes of currents, together with the spatial distribution of the percentage of variance explained by them, are shown in Fig. 6. The first mode explains 84.5% of the variance, the second one 7.3% – not surprisingly significantly less than the first modes of water levels (see Table 3). Moreover, the remaining part of the variance is more regularly distributed among the further modes than in the case of water levels, e.g., as many as 40 modes are necessary to reproduce 98% of the total variance.

The first, most energetic mode (Fig. 6a) reflects mainly the flow in the tidal channels, where it explains over 90% of the variance. In the open sea region to the north of the islands almost all the variance is distributed among the two leading modes (Fig. 6a–d). The further modes are important only locally, mainly over the tidal flats. It must be remembered that these are the locations where large parts of the data consist of zero values (some of the points are flooded only at spring tides and/or during strong wind events). In the case of the currents the influence of drying and flooding is understandably higher than in the case of water levels: shortly before a given location falls dry and shortly after it is flooded again strong currents are present, resulting in very uneven time series. This fact can, at least partially, explain the scatter of variance among numerous only locally significant modes. One can argue that throwing those further modes away removes from the data some of the distortions that arise due to the flooding/drying scheme (which are never to eliminate entirely from the Delft3D model). To investigate in more detail the influence of drying/flooding on the PCA results we repeated the analysis two additional times, after throwing away all points that remained dry at least 75% (run A) or at least 50% of the time (run B), respectively (as compared to 90% in run 0, the results of which were described so far). The differences between the results of the runs 0 and A were negligible, presumably because the number of points included in run 0 and excluded in run A makes up only 4% of N_p. Interestingly, run B resulted in a slightly different variance distribution among the leading modes, with more variance associated with the first mode and less with the second and third mode. Moreover, the total amount of variance described by the first five modes was only 0.9% higher in run B than in run 0. The loss of variance resulting from the inclusion of the points regularly falling dry can be therefore described as minor.

The spatial distribution of variance reconstructed with the five leading modes reflects the bathymetry of the study area (Fig. 7a): the larger the water depth, the higher the reproduced percentage of variance. The first five modes retain at least 97% of variance in 49.5% of points and at least 90% of variance in 69.8% of points. The

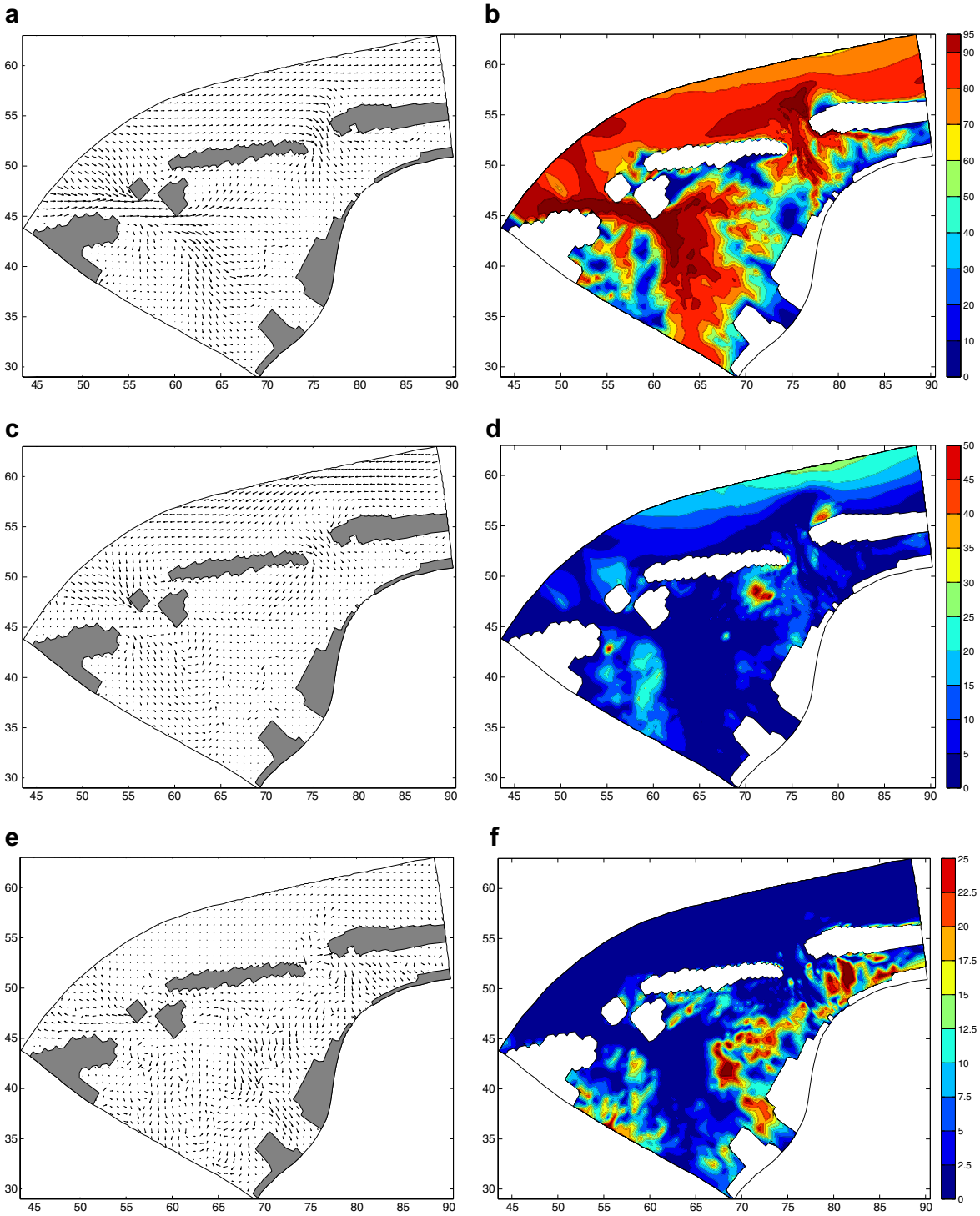

Fig. 6. As in Fig. 3, but for the current velocity data. The arrows have been interpolated onto a regular grid for plotting purposes.

velocities are reproduced within an error of 4–6 cm/s to the north of the islands and 7–10 cm/s over most of the tidal flats (Fig. 7b). The standard deviation of differences between the original and reconstructed time series is lower than 10 cm/s in 95.9% of points.

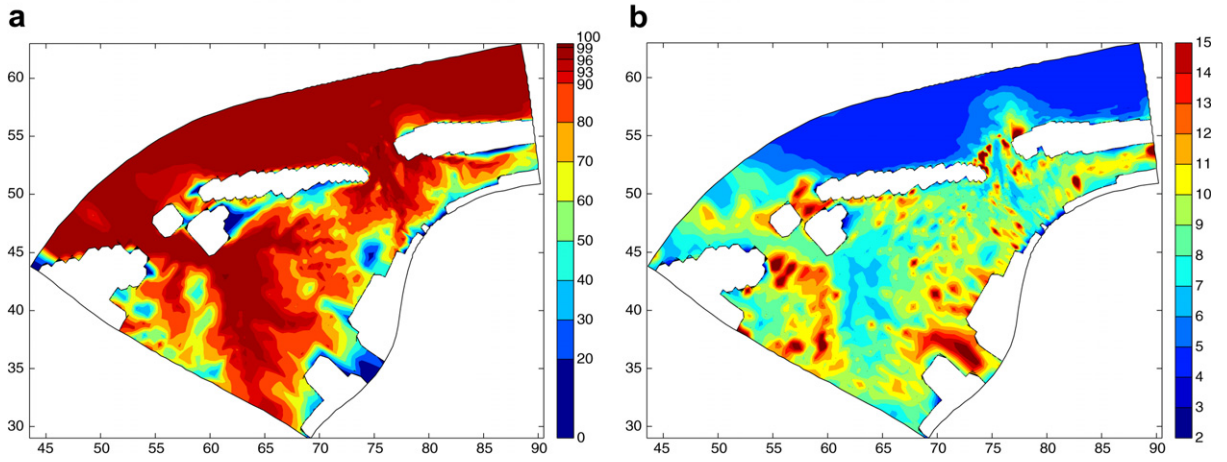

Fig. 7. As in Fig. 4, but for the current velocity data. Standard deviations in cm/s.

Not surprisingly, there is a phase shift of ~90° between $PC_{wl,1}$ – and consequently between the HIPOCAS water level (recall Fig. 5a) – and $PC_{cur,1}$, as shown in Fig. 8a. However, the points are broadly scattered around this 'ideal' path, suggesting high sensitiveness of the currents even to small changes of the forcing, which are practically insignificant for the water levels. This (well known) phenomenon – present in the phase diagrams of the data as well (see Herman, 2007a) – lets expect that the prediction of currents by means of the methods discussed in this paper is more challenging than the prediction of water levels; further on it will be shown that this is the case. Similarly as in the case of water levels, the time variability associated with the three leading modes reveals a dominating tidal modulation (Fig. 8b and c). $PC_{cur,3}$ has twice the tidal frequency, similarly as $PC_{cur,4}$ and $PC_{cur,5}$ (not shown). Interestingly, $PC_{cur,3}$ shifts to a different pattern during extreme wind conditions, when it exhibits a time variability strongly linearly correlated with $PC_{cur,1}$ (days 0–40 in Fig. 8b and c). More details concerning the influence of wind on the PCs of currents will be given in Section 6.

5. Neural network modelling of the tidal dynamics

The NN architecture used here is the multi-layer perceptron (MLP), consisting of two layers of weights providing full connection from the input units to the hidden units and from the hidden units to the output units. Thus, it is a so-called two-layer feed-forward network with error gradient backpropagation as a learning procedure. Basics of NNs can be found in a number of textbooks (e.g. Wu, 1993; Hagan et al., 1995) and will not be discussed here. All simulations presented further have been performed with the `NETLAB` package of MATLAB scripts developed by Nabney (2004). Some of the most important parameters of the MLP used in this study are: hyperbolic tangent activation function of the hidden layer, linear activation function of the output layer (most appropriate choice for nonlinear regression problems) and conjugate gradient optimization algorithm, see Nabney (2004) for details. Other optimization algorithms (scaled conjugate gradient and quasi-Newton), as well as other network architectures (three-layer MLP with and without direct connections from the input layer to the output layer and Elman networks) have been tested, but gave worse results and/or made the training difficult and time consuming. They are therefore not considered further.

After numerous tests the number of hidden units N_h has been set to 60 in both the water levels and the currents NN. Further increase of N_h brought no improvement to the results. As candidates for input parameters to the networks the HIPOCAS water levels ξ and wind velocity components $[U_w, V_w]$ in the point marked with a star in Fig. 1 in the time range from $t - 3\Delta t$ to t (with $\Delta t = 1$ h) have been considered. Additionally, in the case of the currents NN tests have been made with PCs of water levels as input. From a number of over 20 networks with different combinations of the number of input neurons and of the input parameters, the following set gave the best results (in terms of the correlation coefficients σ_r and standard deviation of differences σ_d between the original and modelled PCs) for the water levels NN:

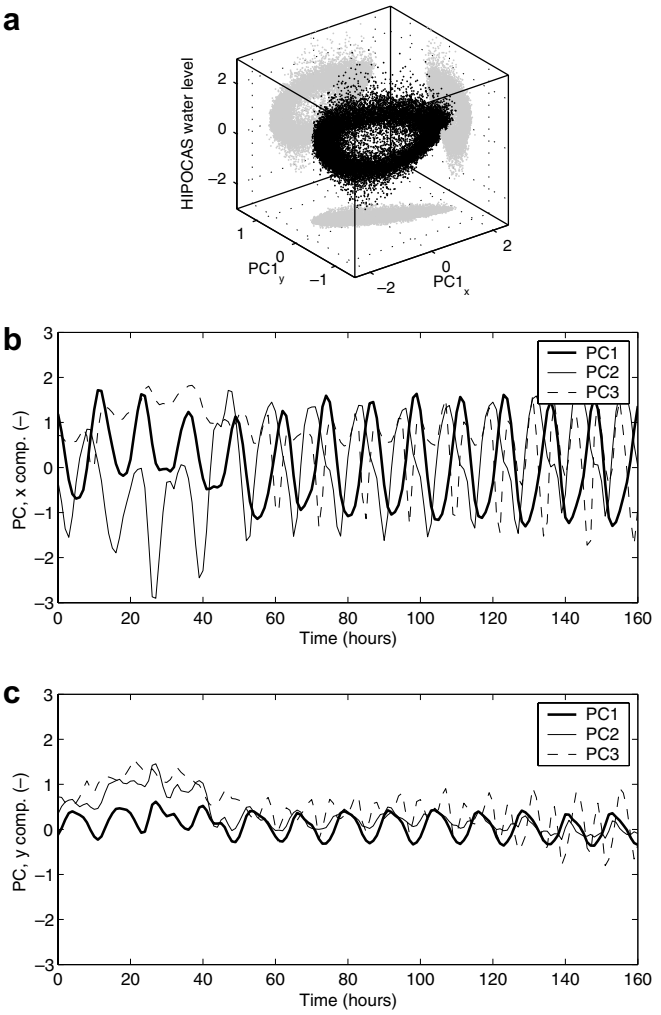

Fig. 8. (a): Dependence of the first PC of currents on the HIPOCAS water level in the point marked with a star in Fig. 1. The gray dots show the projection of the black dots onto the planes of the coordinate system. (b, and c): Fragments of the x- and y-components, respectively, of the first three leading PCs of currents.

$$[\xi(t-2\Delta t),\quad \xi(t-\Delta t),\quad \xi(t),\quad U_{\mathrm{w}}(t),\quad V_{\mathrm{w}}(t), \overline{U}_{\mathrm{w}}(t),\quad \overline{V}_{\mathrm{w}}(t)].$$

For the currents NN the optimal input vector turned out to be:

$$[\xi(t-3\Delta t),\quad \xi(t-2\Delta t),\quad \xi(t-\Delta t),\quad \xi(t),\quad U_{\mathrm{w}}(t),\quad V_{\mathrm{w}}(t),\quad \overline{U}_{\mathrm{w}}(t),\quad \overline{V}_{\mathrm{w}}(t),\quad \mathrm{PC}_{\mathrm{wl},2}(t),\quad \mathrm{PC}_{\mathrm{wl},3}(t)],$$

where $[\overline{U}_{\mathrm{w}}, \overline{V}_{\mathrm{w}}]$ is the 4-h average of $[U_{\mathrm{w}}, V_{\mathrm{w}}]$ (from $t-3\Delta t$ to t). Thus, $N_{\mathrm{i}}=7$ and $N_{\mathrm{i}}=10$ input units have been used for the modelling of water levels and currents, respectively. The last two input neurons of the currents NN contain the 2nd and 3rd PC of water levels, $\mathrm{PC}_{\mathrm{wl},2}$ and $\mathrm{PC}_{\mathrm{wl},3}$. Fig. 5a helps to understand why $\mathrm{PC}_{\mathrm{wl},1}$ brought no improvements to the network performance during tests and why it has not been used as an input parameter in the finally chosen, 'best' network: $\mathrm{PC}_{\mathrm{wl},1}$ is practically a copy of the fourth input neuron ξ.

The output of the networks was:

$$[\mathrm{PC}_{\mathrm{wl},1}(t), \ldots \mathrm{PC}_{\mathrm{wl},5}(t)]$$

and

$$[\mathrm{PC}_{\mathrm{cur},1,x}(t),\ldots\mathrm{PC}_{\mathrm{cur},5,x}(t),\mathrm{PC}_{\mathrm{cur},1,y}(t),\ldots\mathrm{PC}_{\mathrm{cur},5,y}(t)],$$

respectively, resulting in $N_o = 5$ of output units in the case of water levels and $N_o = 10$ in the case of currents. The dataset 1962–1963 has been divided into the training data (January 1962–June 1963) and the validation data (July–December 1963). Tests have shown that the proportion 75% of the data for training and 25% for validation is in this case optimal and that the choice of a particular period for training/validation is not important. By selection of the finally accepted networks from the test ensemble their ability to reproduce the validation data accurately (highest possible σ_r and lowest σ_d) was the only criterion considered. Other features, like e.g., the time needed for training or the learning rate, were considered less important – especially in view of the fact that the behaviour of the tested networks in terms of those criteria varied only slightly (e.g., not a single one from the networks required more than an hour to train and the final values of the cost function lied within 10% of each other).

5.1. NN modelling of water levels

The performance of the trained NN for water levels for the test dataset is shown in Fig. 9 as scatter plots of the five leading PCs. All PCs have been reconstructed with a very high accuracy; the correlation coefficients σ_r are all higher than 99.6%, σ_d vary from 0.021 for the first PC to 0.08 for the fifth PC (see Table 4). When judging the performance of the NN it must be remembered that, although all PCs have a unit standard deviation, they are responsible for very different amount of variance of the original dataset (Table 3). Consequently, it is of fundamental importance to simulate $\mathrm{PC}_{\mathrm{wl},1}$ with the highest possible accuracy. The reconstruction errors of the higher PCs are less relevant for the quality of the reconstructed data.

An important fact is that the PCs can be simulated accurately in the whole range of their values; Fig. 9 shows that the NN copes well not only with 'typical' events, but with 'extreme' ones (up to ±4 standard deviations) as well – although the amount of such events in the training dataset is very limited.

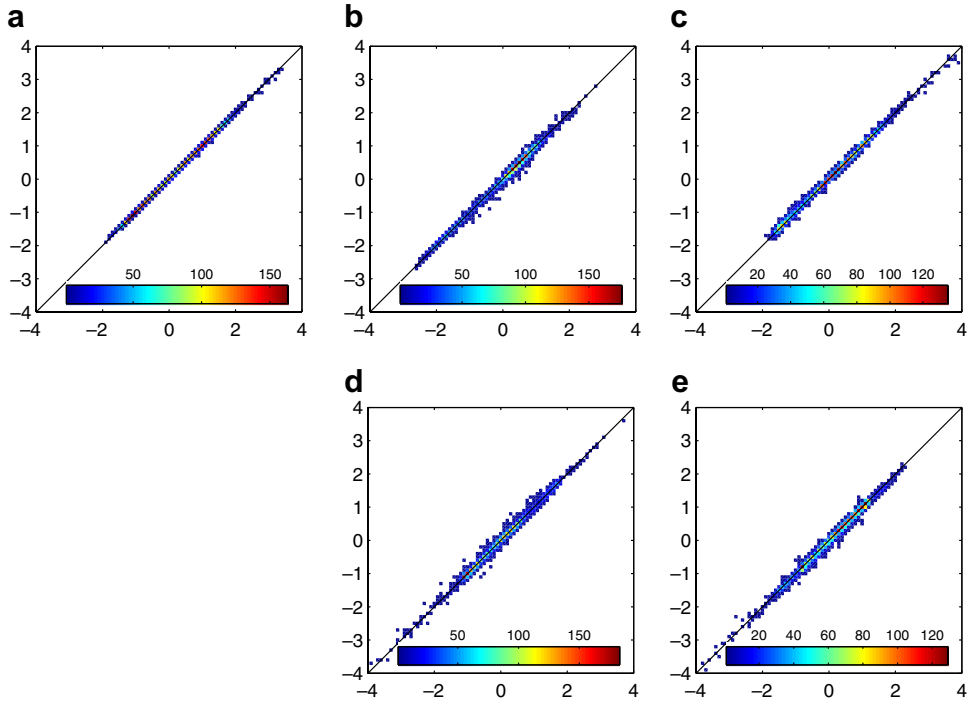

Fig. 9. Scatter plots of the five leading original (horizontal axis) and reconstructed with the NN (vertical axis) PCs (a–e) of water level in the period July–December 1963.

Table 4
Statistical parameters describing the NN performance for the water level test dataset July–December 1963

	$PC_{wl,1}$	$PC_{wl,2}$	$PC_{wl,3}$	$PC_{wl,4}$	$PC_{wl,5}$
Corr. coef. (%) σ_r	99.98	99.74	99.83	99.69	99.64
Std. dev. of differences σ_d	0.021	0.069	0.059	0.072	0.081
Mean difference	0.004	0.018	−0.009	0.002	0.020

When simulating water levels with the technique proposed in this study, there are more sources of errors than the above described inaccuracies in reconstructing the PCs. Firstly, the spatial modes calculated for the 1962–1963 data represent only approximately the variability of the data from other time periods. Secondly, there are only five PCs available, leading to errors analogical to those presented in Fig. 4 for the Delft3D results. Nevertheless, the procedure leads to very satisfactory results, as Fig. 10 shows for the years 1985 and 2002. The reconstructed data represents at least 98% of the variance of the Delft3D results in 88.4% of points in the year 1985 and in 88.1% of points in the year 2002. In majority of points the standard deviation of differences between the original and reconstructed data is lower than 7 cm. A very important fact is that the quality of the results is very similar in both years analyzed, indicating that a similar accuracy can be expected

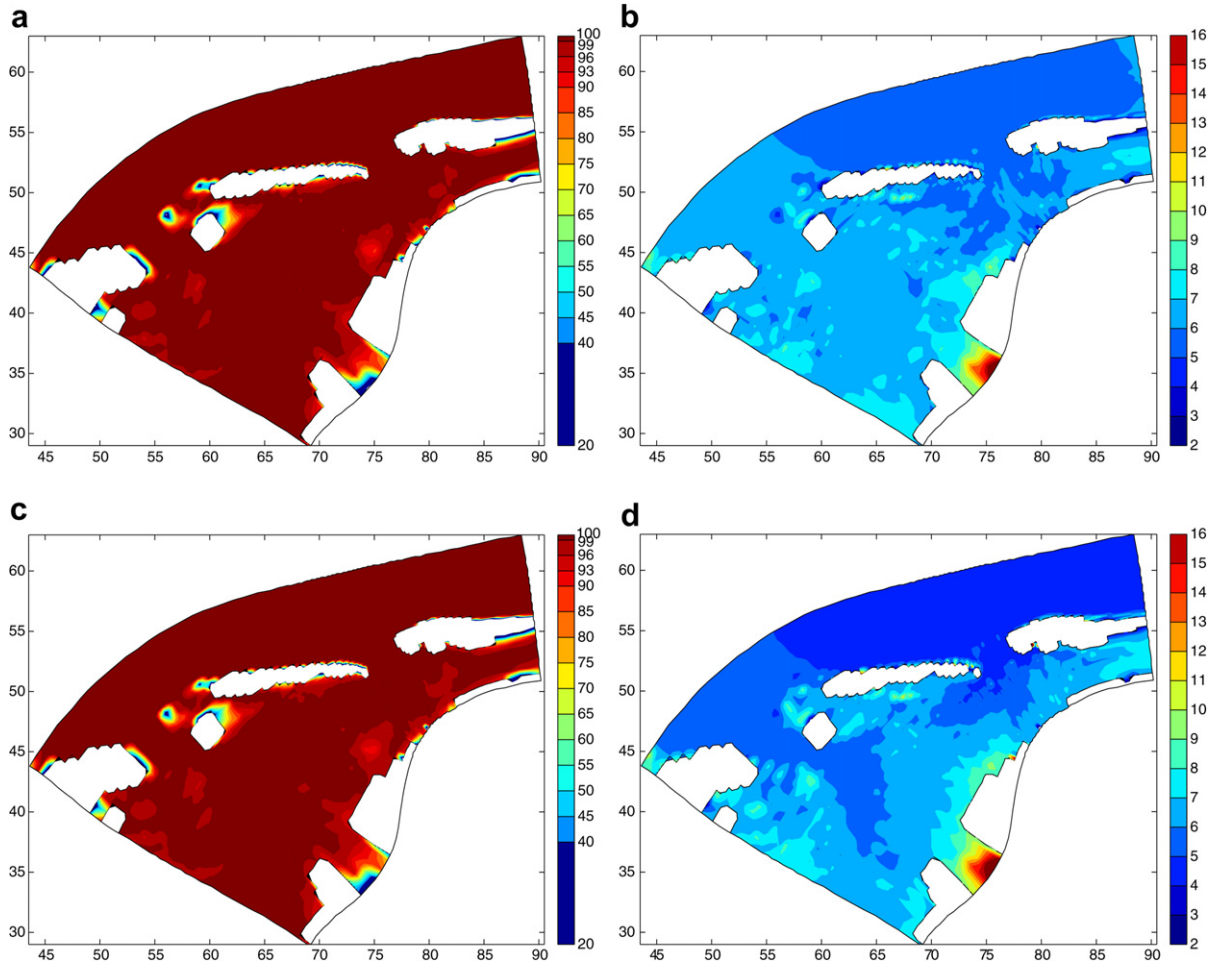

Fig. 10. Performance of the NN model for the water level data from the year 1985 (a and b) and 2002 (c and d): spatial distribution of the percentage of variance reconstructed with the NN (a and c) and of the standard deviation of differences (in cm) between the original and reconstructed data (b and d). Axes labelling in km.

when applying this approach to other time periods (although the patterns in Fig. 10b and d are not the same, the differences do not exceed 1 cm anywhere).

Another measure of the performance of the NN modelling is its ability to reproduce the statistical distribution of the modelled quantities. This ability was investigated in a number of locations in the study area. The results in four of these locations (marked with numbered points in Fig. 1) are shown in Supplementary Fig. 1. Although the NN fails to reproduce some of the small-scale variations in the Delft3D-modelled discrete probability density curves (present particularly at water levels below 0 m), the NN-modelled curves agree well with their Delft3D-modelled counterparts. Moreover, the agreement is satisfactory in all analyzed locations, including the one which falls dry at low water. Similar results were obtained for other analyzed locations, not shown in the diagrams, as well.

5.2. NN modelling of currents

The NN modelling of currents is, not surprisingly, more demanding than the modelling of water levels. Although $PC_{cur,1}$, containing 84.5% of the total variance, has been reconstructed with high accuracy – the standard deviation of differences between the original and reconstructed time series equals 4.1% and 5.6% (for the *x*- and *y*-component, respectively), the correlation coefficient 99.93% and 99.87% – the modelling errors of the further PCs are higher, see Table 5 and Figs. 11 and 12. The scatter of the NN-predicted time series is particularly high for $PC_{cur,3}$ and $PC_{cur,5}$ (Fig. 11c and e and Fig. 12c and e).

The spatial distribution of the reconstructed variance of the currents from the years 1985 and 2002 and of the standard deviation of differences between the Delft3D and the NN results is shown in Fig. 13. The distribution of both parameters reflects the bottom topography of the study area: the higher the water depth, the higher the percentage of the reconstructed variance and the lower the standard deviation of differences (see also Fig. 14). The last parameter varies from 3–6 cm/s seawards from Juist and Norderney to 6–9 cm/s in the tidal channels and 10–15 cm/s over the tidal flats. It is not surprising if one considers that this pattern was already present in the PCA results in Fig. 7. As can be seen in Fig. 14a, within the mean tidal range the percentage of the reconstructed variance decreases almost linearly with the local depth.

The discrete probability density curves for the components of the current velocity show much higher variability from point to point than the corresponding curves for water levels (Supplementary Fig. 2). Nevertheless, this variability has been remarkably well reproduced with the NN in all analyzed locations.

6. Influence of wind on water levels and currents

The properties of the modes and PCs of water levels and currents described so far suggest the dominance of the tidal processes over meteorological forcing in the study area. However, it is well known that the local wind conditions – especially by stable wind direction and/or high wind speeds – can significantly modify the temporal and spatial water level and current patterns in tidal basins, as studied recently e.g., by Herman (2007b) for the tidal inlet Norderneyer Seegat and its surroundings. It was stressed before that PCA tends to scatter physical patterns among a number of modes, making the physical interpretation of its results prob-

Table 5
Statistical parameters describing the NN performance for the currents test dataset July–December 1963

	$PC_{cur,1}$	$PC_{cur,2}$	$PC_{cur,3}$	$PC_{cur,4}$	$PC_{cur,5}$
x-components					
Corr. coef. (%) σ_r	99.93	99.41	91.98	98.11	81.49
Std. dev. of differences, σ_d	0.039	0.109	0.374	0.198	0.503
Mean difference	0.004	−0.004	0.014	0.018	−0.003
y-components					
Corr. coef. (%), σ_r	99.87	98.99	90.49	98.44	76.01
Std. dev. of differences, σ_d	0.053	0.149	0.418	0.195	0.582
Mean difference	0.000	−0.007	−0.021	−0.015	0.013

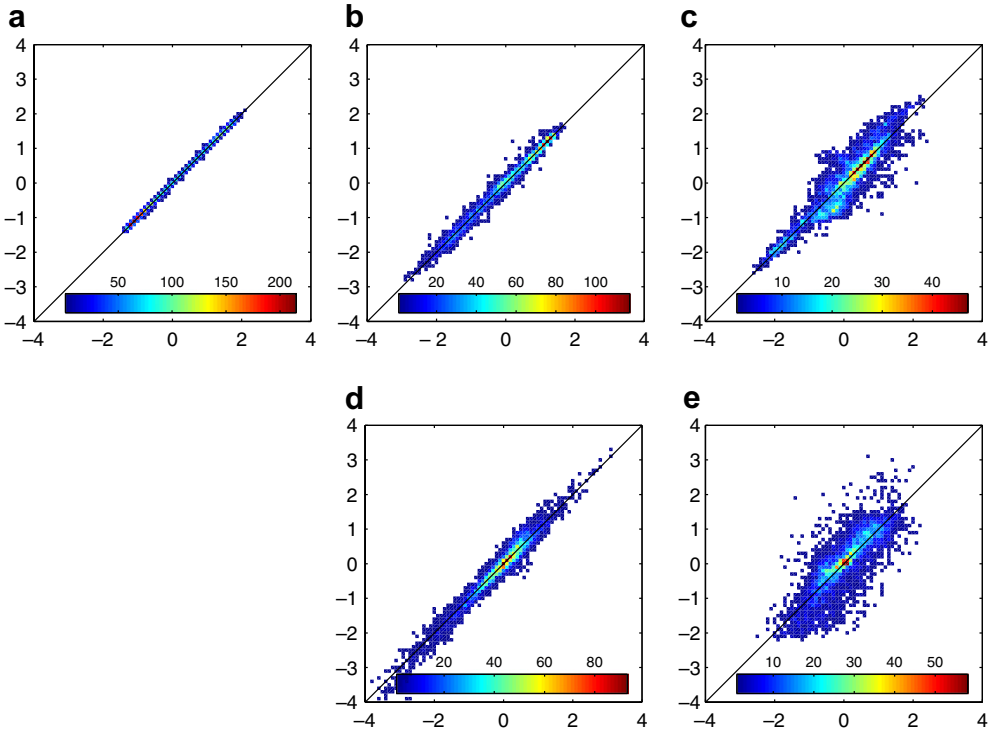

Fig. 11. As in Fig. 9, but for the x-components of the leading PCs of currents.

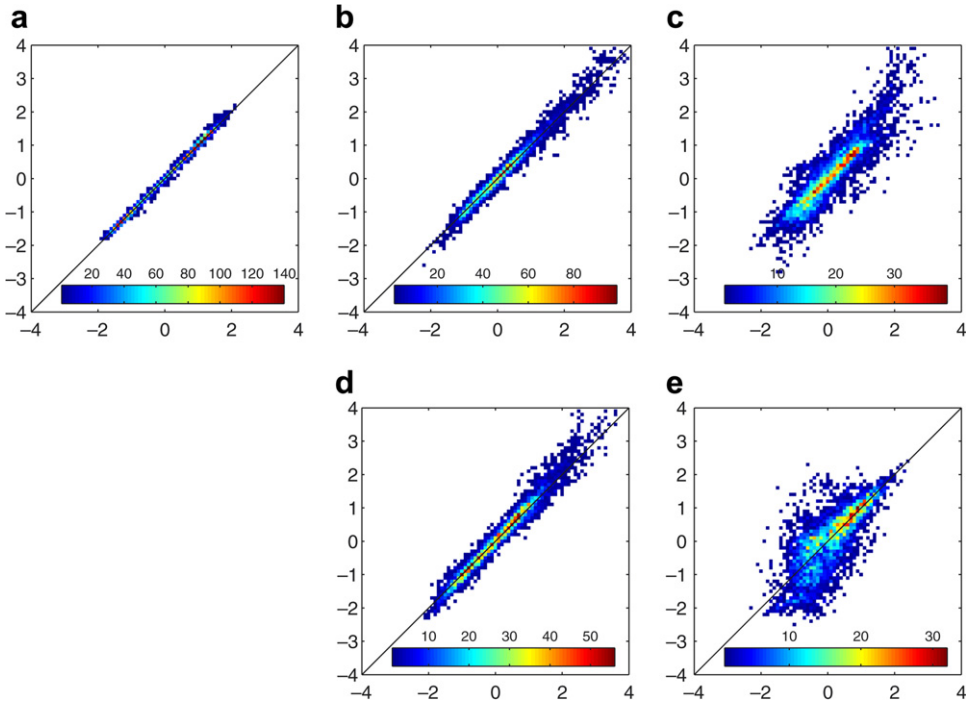

Fig. 12. As in Fig. 9, but for the y-components of the leading PCs of currents.

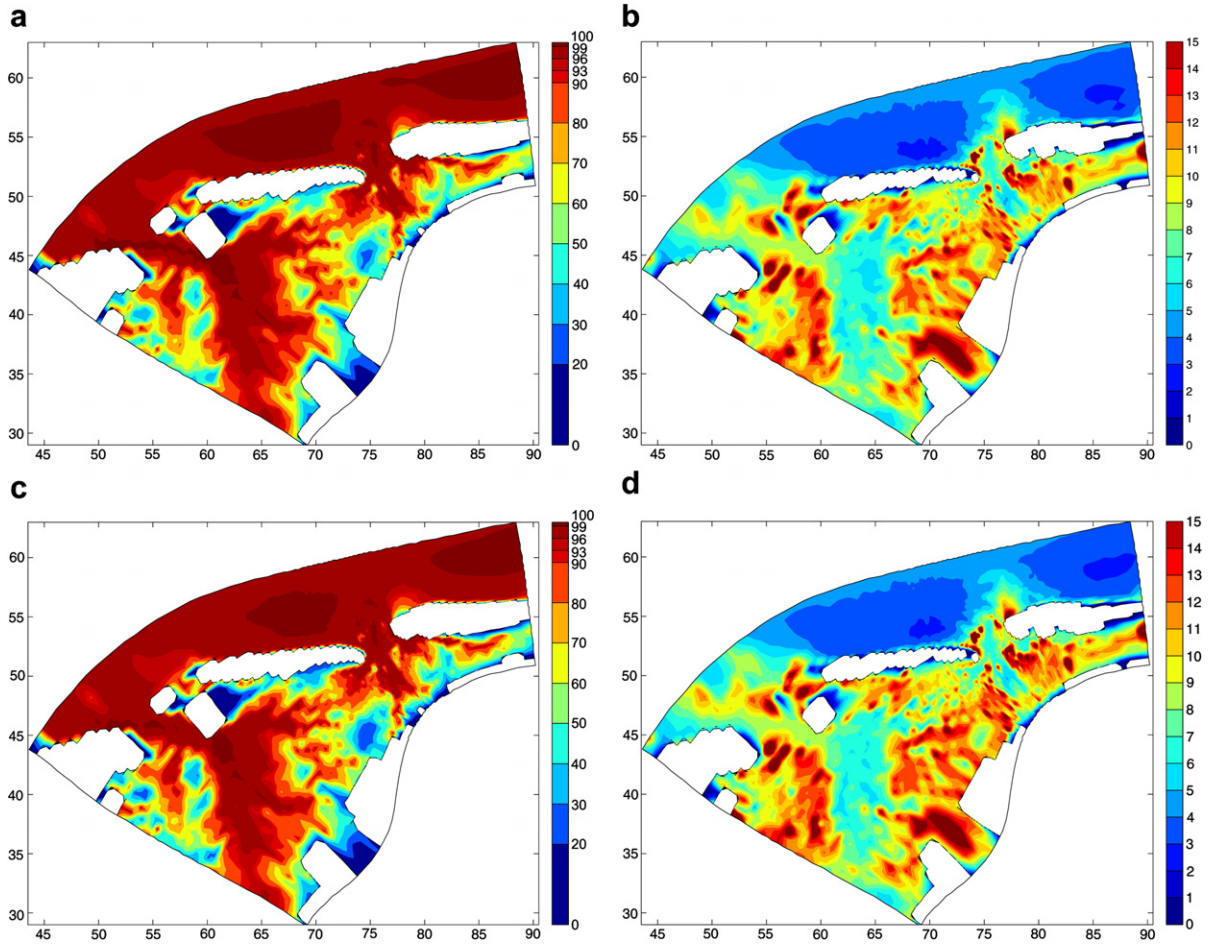

Fig. 13. As in Fig. 10, but for the currents data. Standard deviations in cm/s.

lematic. Nevertheless, it is tempting to undertake some analysis concerning the way in which the wind influence manifests itself in the modelling results. Generally, this influence consists of two parts: the 'external' one, related to the influence of wind and atmospheric pressure on the large scale water level variations in the North Sea and acting on the study area through the open boundary conditions, and the 'internal' one, related to the direct action of wind within the study area. One of the numerous possible approaches towards this analysis could be to run the model without wind two additional times: with realistic boundary conditions (to estimate the 'internal' part) and with astronomical boundary conditions (to estimate the 'external' part). Another straightforward approach toward this issue – justified by the linear nature of PCA – is to remove the tidal signal from each of the PCs ($PC_{wl,i}$ and $PC_{cur,i}$, $i = 1, \ldots, 5$) and to investigate the properties of the residual time series. Let $PC_{wl,t,i}$ and $PC_{cur,t,i}$ denote the time series reconstructed based on the amplitudes and phases of the 25 most energetic tidal components, estimated for $PC_{wl,i}$ and $PC_{cur,i}$, respectively, with the `T_TIDE` package by Pawlowicz et al. (2002). We will analyze the properties of the 'residual' time series $PC_{wl,r,i} = PC_{wl,i} - PC_{wl,t,i}$ and $PC_{cur,r,i} = PC_{cur,i} - PC_{cur,t,i}$ in the context of two quantities: non-tidal component ξ_r of the HIPOCAS water level variations ξ in the point marked with a star in Fig. 1 and the time series of the wind velocity components in this point. The time series $\xi_r = \xi - \xi_t$, where ξ_t denotes the tidal part of ξ obtained with `T_TIDE` analogously to $PC_{wl,t,i}$ and $PC_{cur,t,i}$.

As stated in Section 3, there are no trends in the HIPOCAS data. This is true if the hourly values are considered: the linear trend equals only about 10 cm/s per decade for wind speeds and −0.3 cm per decade for water levels. However, the analysis of the yearly and seasonal mean wind speed values reveals an interesting

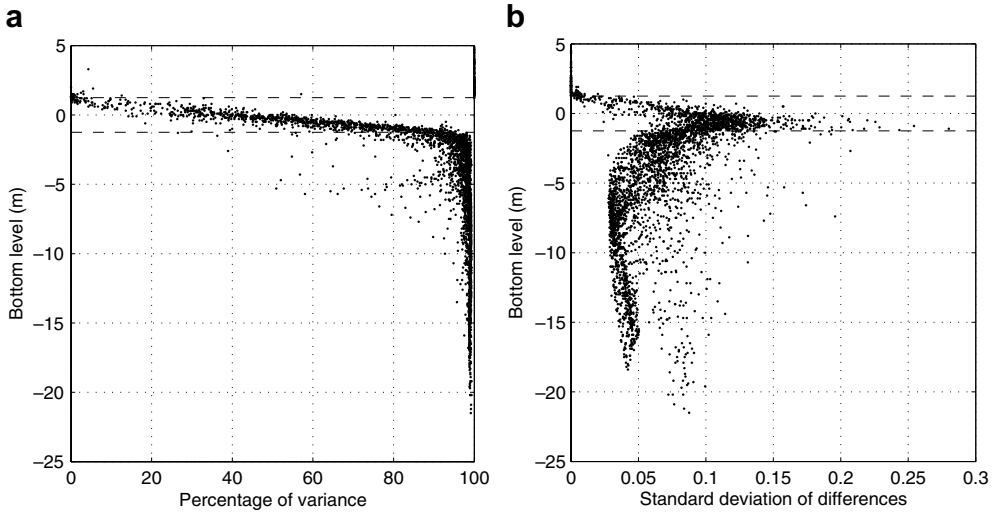

Fig. 14. Dependence of the percentage of the reconstructed variance (a) and of the standard deviation of differences between the original and reconstructed current data (b; in cm/s) on the bottom level. All points within the study area are plotted. Dashed lines mark the mean tidal range.

feature (Fig. 15). In the four decades studied the winds became slightly weaker in the summer (June–August) and markedly stronger in winter (December–February), resulting in a positive trend for the yearly-mean wind speeds. This phenomenon is related to increasing occurrence frequency of strong wind events in the cold time of the year. Another important feature is the seasonal variability of wind speed and direction – and the resulting variability of water level residual ξ_r – which manifests itself in the differences of 2–3 m/s in the average winter and summer wind speeds (Fig. 15), as well as in the distributions presented in Fig. 16. Most strong wind events with winds above 15 m/s take place in winter. They are associated with low pressure systems passing typically in an approximately easterly direction to the north of the study area. Thus, during storms the wind shifts gradually from SW through W to NW. Strong easterly winds are rare. The most frequent wind direction in winter (WSW) does not deviate much from the annual average (the dominance of WSW winds, which is an offshore direction in the study area, can partly explain the lack of trend of the wintertime mean water levels, that one could expect to accompany the increasing wind speeds shown in Fig. 15); in the summer the

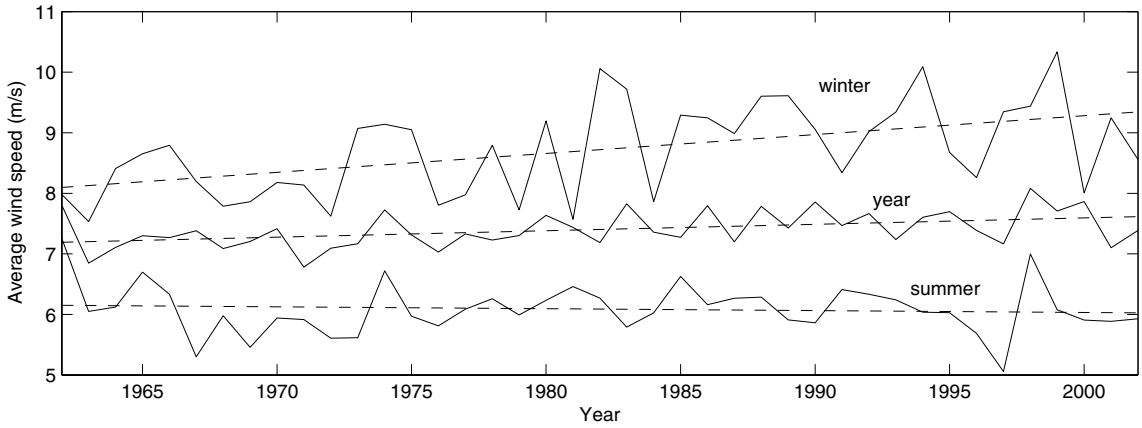

Fig. 15. Time series of yearly, wintertime (December–February) and summertime (June–August) mean wind speed (in m/s) from the HIPOCAS dataset (point marked with a star in Fig. 1).

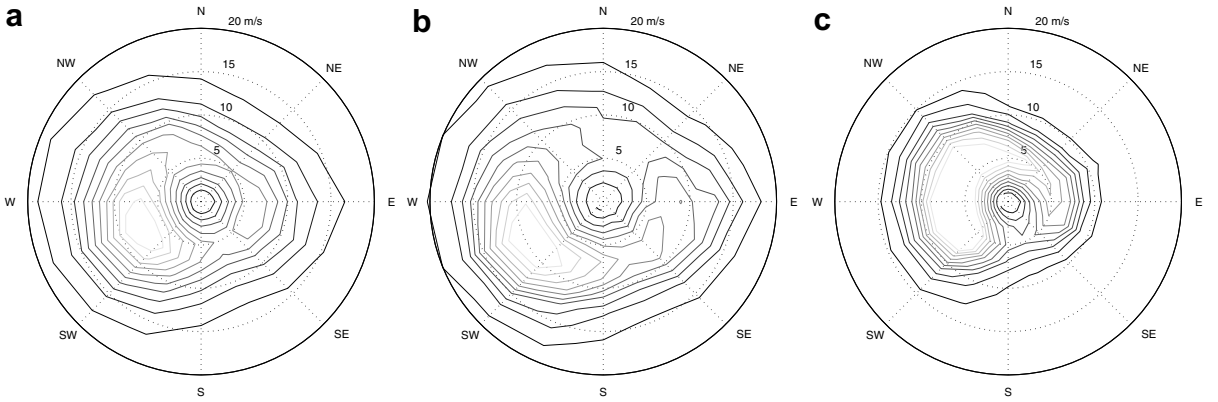

Fig. 16. Two-dimensional histograms of HIPOCAS wind velocity (class width 2 m/s and 22.5°) in the point marked with a star in Fig. 1 in an average year (a), winter (b) and summer (c). Data from the period 1962–2002.

dominating wind directions are broadly scattered between SW and NW; southeasterly winds are untypical for this time of the year (Fig. 16c).

In view of these properties of the wind distribution it is interesting to notice the existence of the 'dominating' wind direction if the variability of ξ_r and $PC_{wl,r,1}$ is concerned. The dependence between these quantities and the wind speed is limited to a relatively narrow directional sector centered approximately around an WNW–ESE axis. Let denote the component of the wind velocity vector along this axis by u_w and the component perpendicular to this axis by v_w:

$$[u_w, v_w] = U_w[\cos\alpha, -\sin\alpha] + V_w[\sin\alpha, \cos\alpha]$$

with $\alpha = -20°$. The relationship between u_w and $PC_{wl,r,1}$ (Fig. 17a) and ξ_r (not shown) is approximately quadratic (presumably a consequence of a quadratic friction term applied in the model at the free surface), with the linear correlation coefficient between $\mathrm{sign}(u_w)u_w^2$ and $PC_{wl,r,1}$ equal to 86% and between $\mathrm{sign}(u_w)u_w^2$ and ξ_r equal to 85.6%. No statistically significant correlation could be found for the v_w component or its polynomials (Fig. 17b). It can hardly be a coincidence that exactly the WNW winds are known to produce the highest 'effective' wind speeds and thus to result in the highest storm surges along the southern North Sea coast. This phenomenon is related to the larger-scale processes, as the above results clearly demonstrate: the u_w-forcing is

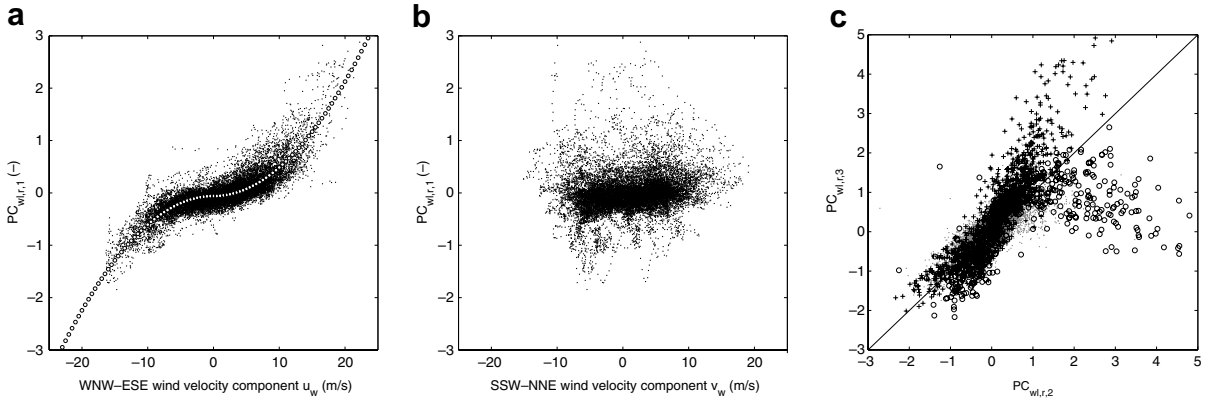

Fig. 17. Scatterplots of $PC_{wl,r,1}$ versus u_w (a), $PC_{wl,r,1}$ versus v_w (b) and $PC_{wl,r,3}$ versus $PC_{wl,r,2}$ (c). Circles in (a) show the best linear fit between $\mathrm{sign}(u_w)u_w^2$ and $PC_{wl,r,1}$. Circles and crosses in (c) correspond to $u_w \leqslant -10$ m/s and $u_w \geqslant 10$ m/s, respectively; the remaining points (for $|u_w| < 10$ m/s) are shown in gray.

Table 6
Variance of $PC_{wl,r,i}$ and $PC_{cur,r,i}$ (in percent of the variance of $PC_{wl,i}$ and $PC_{cur,i}$, respectively). Y = year, W = winter (December–February), S = summer (June–August)

PC	Water level			Current, x-components			Current, y-components		
	Y	W	S	Y	W	S	Y	W	S
1	12.8	21.5	4.1	2.0	3.2	0.9	6.0	9.7	2.5
2	20.5	32.3	8.7	12.6	19.1	5.5	72.3	82.5	50.1
3	25.1	37.4	12.1	26.3	35.5	16.6	49.4	62.9	29.9
4	63.3	77.1	38.7	78.1	85.7	60.1	46.3	59.4	27.8
5	74.4	85.1	53.7	35.7	46.3	23.0	42.4	53.8	27.7

present already in the boundary data (through ξ_r) and is without significant transformations transferred to $PC_{wl,r,1}$ (recall Fig. 5a). Thus, $PC_{wl,1}$ and the associated mode (Fig. 3a) are responsible for the water level variations inside the study area resulting from both the tidal forcing and the wind surge present in the boundary conditions. The variance of $PC_{wl,r,1}$ constitutes 12.8% of the overall variance of $PC_{wl,1}$, with increased percentage in the winter months (21.5%) and decreased in the summer months (4.1%), see Table 6.

The interpretation of the role of $PC_{wl,r,2}$ and $PC_{wl,r,3}$ is less straightforward. Fig. 17c shows a scatterplot of these time series for various wind conditions. Generally, for $u_w > 0$ ($u_w < 0$) we have $PC_{wl,r,3} > PC_{wl,r,2}$ ($PC_{wl,r,3} < PC_{wl,r,2}$). Also, it can be shown that the highest $PC_{wl,r,2}$ ($PC_{wl,r,3}$) values occur at low (high) tide – which is not surprising if one examines the spatial modes in Fig. 3c and e. The role of the second and third mode over the tidal flats is to compensate for low values of the first mode at shallow locations (Fig. 3a). At high water levels this can be done better with the third mode (with its positive values seawards from the islands); at low water levels – with the second mode (with its negative values seawards from the islands). The effect is of course strongest at times with high tide accompanied with positive u_w and low tide accompanied with negative u_w. Similarly to $PC_{wl,r,1}$, the percentage of the non-tidal variance of the further components is significantly higher in winter than in summer (Table 6). Also, the further modes/PCs reflect mainly the 'internal' (local) part of the wind forcing, contrary to $PC_{wl,r,1}$, which reflects mainly the 'external' part (the variability of ξ_r).

In the case of currents the situation is similar – with an analogous seasonal variation of the percentage of variance of $PC_{cur,r,i}$ relative to $PC_{cur,i}$ (Table 6), strong dependence of $PC_{cur,r,1}$ on u_w (not shown) etc. – but the detailed interpretation of the PCs is more complicated, partly because the complex modes must be multiplied by the complex PCs to obtain meaningful current patterns. Herman (2007b) showed that the presence of wind can drastically change these patterns and momentary water transport through the boundaries of the tidal

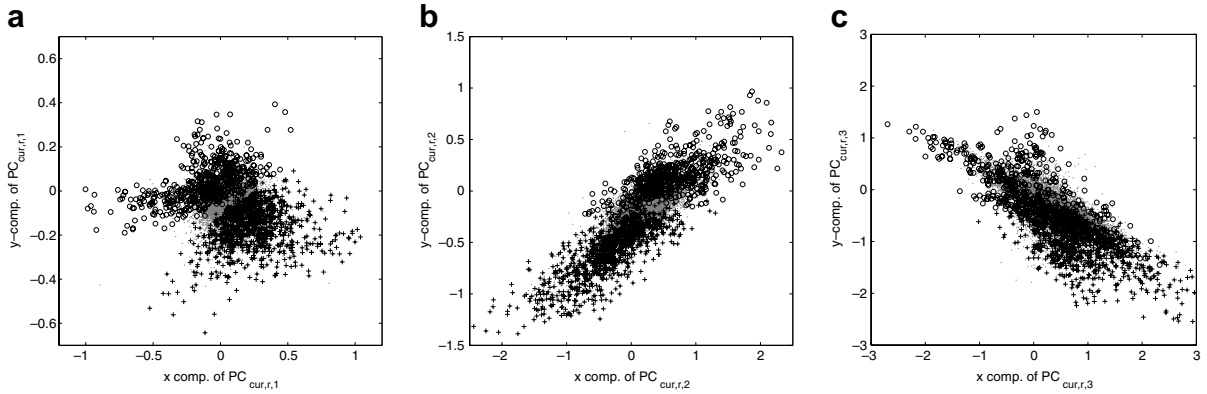

Fig. 18. Scatterplots of y- versus x-components of $PC_{cur,r,1}$ (a), $PC_{cur,r,2}$ (b) and $PC_{cur,r,3}$ (c). Circles and crosses correspond to $u_w \leqslant -10$ m/s and $u_w \geqslant 10$ m/s, respectively; the remaining points (for $|u_w| < 10$ m/s) are shown in gray.

basins under study. E.g., during extreme storm surges generated by westerly winds the wind-generated currents in the Wadden Sea can strongly reduce or even totally reverse the direction of the flood current in the Norderneyer Seegat (Koch and Niemeyer, 1977). The wind has also an indirect influence on the spatial current distribution, e.g., easterly winds lead to lower water levels in the study area, thus increasing the role of the bottom topography upon the circulation regime. In Fig. 18 the dependence of $PC_{cur,r,1}$, $PC_{cur,r,2}$ and $PC_{cur,r,3}$ on u_w is shown. For positive (negative) u_w the action of $PC_{cur,r,1}$ upon the first mode of currents (Fig. 6a) is to direct the flow through the inlets between the islands to (from) the Wadden Sea. Also, by high positive u_w the non-tidal parts of $PC_{cur,1}$ and $PC_{cur,2}$ tend to decrease (increase) the cross-inlet water transport in the Norderneyer Seegat during flood (ebb). An examination of $PC_{cur,r,3}$, which plays an important role over the tidal flats (Fig. 6f), reveals that the current direction in shallow locations corresponds to the local wind direction. The variability of $PC_{cur,r,3}$ is responsible for the specific behaviour of $PC_{cur,3}$ during strong wind events, pointed out in Section 4 (Fig. 8b and c); at high water $PC_{cur,r,3}$ directs the flow over the flooded shallows in the wind direction. Generally, the role of the non-tidal part of currents is higher seawards from the islands and in the tidal channels, where the water depth is high enough for the wind-driven circulation to develop.

7. Summary and discussion

Medium-term modelling of hydrodynamic processes in shallow coastal seas is a difficult and computationally expensive task. An effective and accurate approach to the problem has been proposed in this paper, combining the high-resolution hydrodynamic modelling with methods based on the principal component analysis and on neural networks. The main idea behind this approach is the universal character of the spatial patterns of the analyzed quantities (water level and current fields) over time. Although the results of the principal component analysis are – strictly speaking – representative exclusively for the data used to perform this analysis, the repeatable character of the phenomena studied makes it possible to use the same patterns (modes) for various time periods, thus reducing the modelling task to simulating the principal components. A simple feed-forward neural network is sufficient to produce the leading PCs based on input time series of water level and wind in a chosen (single) location. To put it shortly: having a set of spatial modes, a trained NN and time series of input data, one is able to simulate e.g., one year of water level and current fields within seconds – unachievably fast for hydrodynamic modelling (e.g., a one-year-simulation with Delft3D in our study area required two months of calculations on a personal computer). Thus, the approach can be used to obtain water level and current fields of high quality in periods which could not have been modelled with Delft3D because of time constrains. Moreover, the method has been shown to be able to accurately reproduce the statistical distribution of the water levels and currents in the study area, which is of crucial importance for the further application of the results e.g., for the morphodynamic modelling.

There are some issues regarding the results presented in this work that deserve some discussion. One of them concerns the choice of a location used as a source of input data for the NN modelling. The only limitation seems to be that one should use data representative for the general conditions in the study area, e.g., wind measurements from sheltered stations, distorted by the influence of the local topography, should be avoided. The representativeness requirement means also that one can expect a decrease in the performance of the PCA/NN technique with increasing size of the study area (relative to the characteristic dimensions of meteorological and hydrodynamic patterns occurring within it).

Another important issue is the choice of the time period for the PCA. In Section 6 the presence of trends e.g., in the wintertime mean wind speeds was discussed. In spite of that, no relation between the time period selected for PCA and the quality of the NN modelling could be found – a clear indication that the *occurrence frequency* and not the *character* of the strong wind events has changed during the four decades studied. Thus, the quality of the NN modelling remained unaffected by those – for many problems (including morphodynamics) very important – changes.

Finally, it must be stressed that the approach presented in this work gives results of the quality comparable with the one obtained e.g., by Lee and Jeng (2002), Huang et al. (2003) or Lee (2004) for water level modelling

in *single* locations. In spite of the noticeable higher complexity of the problem analyzed here, comparable values of the correlation coefficients and standard deviation of differences could be obtained. If the PCA/NN modelling of currents is concerned, it must be remembered that the results are of high quality when compared with the results of Delft3D; their accuracy with the real-world currents could not be estimated because of the lack of appropriate measurements.

Acknowledgements

The work presented here has been part of the research project MOSES (''Modelling of the medium-term wave climatology at the German North Sea coast''; Project No. 03 KIS 040) financed by the German Federal Ministry for Education and Research (BMBF) under the umbrella of the German Coastal Engineering Research Council (KFKI). We thank our colleagues from the Coastal Research Station for their assistance and support. We also thank the anonymous reviewers for valuable comments and criticism that helped to improve the quality of this paper.

Appendix A. Supplementary data

Supplementary data associated with this article can be found, in the online version, at doi:10.1016/j.ocemod.2007.02.004.

References

Álvarez, A., López, C., Riera, M., Hernández-García, E., Tintoré, J., 2000. Forecasting the SST space-time variability of the Alboran Sea with genetic algorithms. Geophys. Res. Lett. 27, 2709–2713.

Álvarez, A., Orfila, A., Basterretxea, G., Tintoré, J., Vizoso, G., Fornes, A., 2007. Forecasting front displacements with a satellite based ocean forecasting (SOFT) system. J. Marine Syst. 65, 299–313.

Delft Hydraulics, 2001. Flow modelling of East-Frisian Waddensea. Set-up and calibration of tidal flow model. Technical report, Delft Hydraulics.

Delft Hydraulics, 2003. User manual of Delft3D-FLOW: Simulation of multi-dimensional hydrodynamic flows and transport phenomena, including sediments. Technical report, Delft Hydraulics, p. 497.

de Vriend, H.J., Capobianco, M., Chesher, T., de Swart, H.E., Latteux, B., Stive, M.J.F., 1993. Approaches to long-term modelling of coastal morphology: a review. Coastal Engng. 21, 225–269.

Hagan, M.T., Demuth, H.B., Beale, M.H., 1995. Neural Network Design. PWS Publishing Company, Boston, p. 736.

Hayes, M., 1979. Barrier island morphology as a function of tidal and wave regime. In: Leatherman, S.P. (Ed.), Barrier Islands From the Gulf of St. Lawrence to the Gulf of Mexico. Academic Press, New York, pp. 1–29.

Herman, A., 2007a. Nonlinear principal component analysis of the tidal dynamics in a shallow sea. Geophys. Res. Lett. 34, L02608. doi:10.1029/2006GL027769.

Herman, A., 2007b. Numerical modelling of water transport processes in partially-connected tidal basins. Coastal Engng. 54, 297–320.

Huang, W., Murray, C., Kraus, N., Rosati, J., 2003. Development of a regional neural network for coastal water level predictions. Ocean Engng. 30, 2275–2295.

Koch, M., Niemeyer, H.-D., 1977. Storm surges and current measurements in the Norderneyer Seegat area. Forschungsstelle für Insel- und Küstenschutz, Jahresbericht 1977 XXIX, 91–108 (in German).

Lee, T.-L., 2004. Back-propagation neural network for long-term tidal predictions. Ocean Engng. 31, 225–238.

Lee, T.-L., Jeng, D.S., 2002. Application of artificial neural networks in tide-forecasting. Ocean Engng. 29, 1003–1022.

Luijendijk, A.P., 2001. Validation, calibration and evaluation of Delft3D-FLOW model with ferry measurements. PhD thesis, Delft University of Technology, Delft, p. 92.

Nabney, I.T., 2004. NETLAB. Algorithms for pattern recognition. Advances in Pattern Recognition, 4th ed. Springer-Verlag, UK, p. 420.

Niemeyer, H.D., Goldenbogen, R., Schroeder, E., Kunz, H., 1995. Investigations into the morphodynamics of the Wadden Sea in the research project WADE. Die Küste 57, 65–94 (in German).

O'Brien, M.P., 1967. Equilibrium flow areas of tidal inlets on sandy coasts. Proceedings of the 10th Conference on Coastal Engineering. ASCE, New York, pp. 676–686.

Pawlowicz, R., Beardsley, B., Lentz, S., 2002. Classical tidal harmonic analysis including error estimates in MATLAB using T_TIDE. Comput. Geosci. 28, 929–937.

Preisendorfer, R.W., 1988. Principal component analysis in meteorology and oceanography. Elsevier Science, New York, p. 425.

Roelvink, J.A., van Banning, G.K.F.M., 1994. Design and development of Delft3D and application to coastal morphodynamics. In: Verwey, A., Minns A.W. (Eds.), Proceedings of Hydroinformatics 1994, USA, pp. 451–456.

Schroeder, E., Goldenbogen, R., Kunz, H., 1994. 24th Proceedings of the Coastal Engineering. Kobe, Japan, pp. 3251–3265.

Stanev, E.V., Flöser, G., Wolff, J.O., 2003a. First- and higher-order dynamical controls on water exchanges between tidal basins and the open ocean. A case study for the East Frisian Wadden Sea. Ocean Dynam. 53, 146–165.

Stanev, E.V., Wolff, J.O., Burchard, H., Bolding, K., Flöser, G., 2003b. On the circulation in the East Frisian Wadden Sea: numerical modeling and data analysis. Ocean Dynam. 53, 27–51.

Weisse, R., Feser, F., Günther, H., 2002. A 40-year high-resolution wind and wave hindcast for the Southern North Sea. Proceedings of the 7th International Workshop on Wave Hindcasting and Forecasting. Banff, Alberta, Canada, pp. 97–104.

Wu, J.-K., 1993. Neural networks and simulation methods. CRC, New York, p. 456.